Complementary studies of dc arc by experiments and combined modelling of the plasma bulk and the cathode boundary layer

C. Mohsni[1,2], M. Baeva[2], St. Franke[2], S. Gortschakow[2], Z. Araoud[1] and K. Charrada[1].

[1] *National School of Engineering of Monastir, 5000 Rue Ibn Jazzar, Monastir 5035, Tunisia*
[2] *Leibniz Institute for Plasma Science and Technology, Felix-Hausdorff-Str. 2, 17489 Greifswald, Germany*

Abstract: The work is concerned with experimental and modelling studies on dc electric arcs. The configuration consists of a conically shaped tungsten cathode and a graphite anode in a distance of 5 mm. Electrical and spectroscopic measurements are used to obtain the arc voltage and the plasma temperature. A combined modelling approach is developed to extend the equilibrium description of the arc plasma to include the contribution of the non-equilibrium cathode boundary layer. The results obtained clearly show a good agreement.

Keywords: Arc discharge, plasma diagnostics, non-equilibrium boundary layer.

1. Introduction

The modelling of electric arcs, which combines the equilibrium description of the bulk plasma and a non-equilibrium treatment of the near-electrode regions [1, 2], has been considered as an alternative to the fully equilibrium approach applied over the course of many years [3,4] and the fully non-equilibrium approaches suggested in [5,6]. The combined modelling of the plasma bulk and the cathode boundary layer in dc arcs with a refractory cathode allows us to account for the significant amount of electric power deposited in the thin boundary layer adjacent to the cathode, in particular for current below 200 A, and to reduce the discrepancy to the measured arc voltage, and therefore to improve the predictive capability of the model. This modelling approach can be, in general, more easily applied to electric arcs in molecular gases, which are used in industrial devices, e.g. circuit breakers.

In this work, we present results of complementary studies of dc electric arcs, which have been done by electrical and spectroscopic measurements, and a combined modelling of the equilibrium arc plasma and the non-equilibrium cathode boundary layer. On the one hand, the studies are aimed at the model validation; while on the other hand, the model will deliver plasma parameters, which cannot be easily measured. Here, we consider the experimental and modelling studies in argon at atmospheric pressure. Forthcoming works are dedicated to experiments and modelling in Air- and CO_2-gas, which are considered as alternatives to the SF_6-gas in switching applications.

2. Experiment

The experimental setup is shown in Fig. 1. The anode is spherically shaped and made of graphite. The cathode is a cylindrical rod (diameter 2 mm) with a conical tip (40°) and it is made of tungsten. The distance between the cathode tip and the anode is 5 mm. The surrounding gas is argon at atmospheric pressure. The image of the arc is taken by a high-speed video camera of the type IDT Motion Pro Y6. The arrangement is placed inside a chamber. The gas pressure is controlled by a manometer. The arc is ignited making use of a spark coil arrangement.

The equipment for optical emission spectroscopy (OES) consists of a spectrograph Acton SP2500 with a focal length of 0.5 m and an intensified CCD camera Princeton Instruments PI-MAX4. The obtained images contain spectral and spatial side-on information about the arc. The arc is imaged by a spherical mirror on the entrance slit of the spectrometer with a width of 30 µm. Emitted spectra are acquired radially resolved, in the middle between the electrodes. Absolute calibration is performed by a calibrated tungsten strip lamp placed at the position of the arc. The radiation of the Ar I 772 nm line is spectrally resolved using a grating with 150 lines/mm. An integration over the wavelength integral is performed and Abel inversion is done to get the radial dependence of the emission coefficient. The excited state density of the upper level corresponding to the transition of the Ar I 772 nm line is derived. Assuming Local Thermodynamic Equilibrium (LTE), the population density is related to the plasma temperature. From a pre-calculated equilibrium composition of argon, the temperature is obtained.

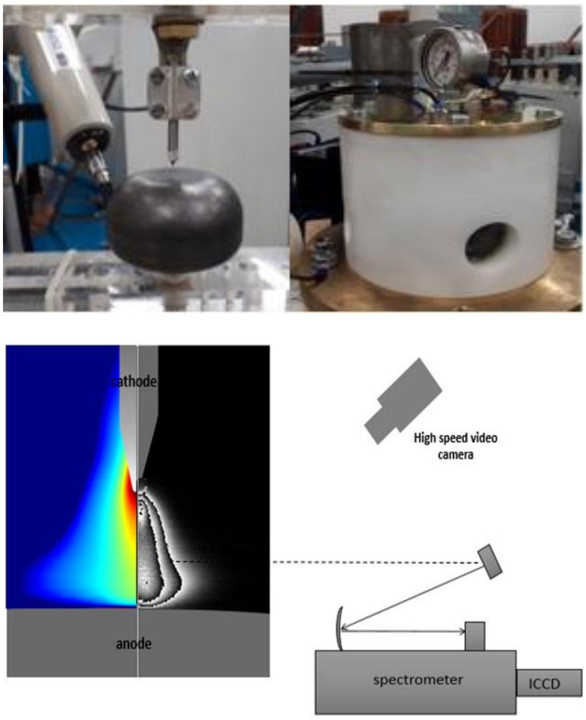

Fig. 1. A view of the experimental arrangement, the spectroscopic equipment and the computational domain.

3. Modelling approach

The combined modelling approach involves the magneto-hydrodynamic (MHD) description of the arc column under the assumption of LTE, the heat and current transfer in the electrodes, and the non-equilibrium boundary layer of the thermionic cathode. The MHD model is coupled through the boundary layer to the electrode.

The MHD description of the arc column is based on the Navier-Stokes equations for conservation of mass, momentum and energy. The gas flow is assumed to be laminar, and the plasma under the assumption of LTE is characterized by a single temperature. A stationary solution is sought for the equations

$$\nabla \cdot (\rho \boldsymbol{u}) = 0, \tag{1}$$

$$\rho(\boldsymbol{u} \cdot \nabla)\boldsymbol{u} = \nabla \cdot \left(-p\hat{I} + \hat{\tau}\right) + \boldsymbol{F}_L, \tag{2}$$

$$\rho C_p(\boldsymbol{u} \cdot \nabla T) + \nabla \cdot \boldsymbol{q} = Q_J - Q_{rad}, \tag{3}$$

where ρ is the mass density, $\boldsymbol{u}$ is the flow velocity, p is the pressure, $\hat{\tau}$ is the stress tensor, $\hat{I}$ is the identity matrix, and $\boldsymbol{F_L}=\boldsymbol{j}\times\boldsymbol{B}$ is the Lorentz force. In Eq. (3), C_p is the specific heat at constant pressure, T is the gas temperature, $\boldsymbol{q}=-\kappa\nabla T$ is the heat flux due to thermal conduction with κ being the thermal conductivity. The gas is heated by Joule heating $Q_J=\boldsymbol{j}\cdot\boldsymbol{E}$, where **j** is the electric current density, and cooled by radiation Q_{rad}.

The Maxwell equations and the Ohm's law are used to obtain the self-induced magnetic field $\boldsymbol{B}$ and the electric potential φ

$$\nabla\times\boldsymbol{B} = \mu_0\boldsymbol{j}, \qquad \mathbf{B} = \nabla\times\boldsymbol{A} \tag{4}$$

$$\nabla\cdot\boldsymbol{j} = 0; \quad \boldsymbol{j} = \sigma\boldsymbol{E} = -\sigma\nabla\varphi \tag{5}$$

The electric field $\boldsymbol{E}$ and the self-induced magnetic field $\boldsymbol{B}$ couple the electromagnetic part of the model to the fluid through the Lorentz force and the Joule heating. The transport properties needed are taken from [7-9].

The heat conduction and current continuity equations are solved in the electrodes:

$$\nabla\cdot(k_s \nabla T)+\boldsymbol{j}\cdot\boldsymbol{E} = 0 \tag{6}$$

$$\nabla\cdot\boldsymbol{j} = 0; \quad \boldsymbol{j} = \sigma_s\boldsymbol{E} = -\sigma\nabla\varphi \tag{7}$$

The electrical conductivity σ_s and the thermal conductivity k_s of the solid materials are taken as a function of the temperature T.

The cathode boundary layer includes the region of space-charge adjacent to the cathode surface (the sheath) and the ionization layer, which is adjacent to the sheath. The energy balance is considered in the boundary layer [10,11] in account for 1) the heat flux leaving the boundary layer and going to the cathode, 2) the electric power density deposited in the boundary layer, 3) the power brought by the electrons emitted from the cathode, and 4) the heat flux entering the boundary layer from the LTE plasma. This energy balance along with the total current density expressed as the sum of the density of the thermionic emission current (j_{em}), the ion current density (j_{ion}), and the density of electric current transported by counter-diffusing electrons (j_{be}), determines the heat flux q and the current density j_w on the cathode surface as functions of the voltage drop U_{tot} in the boundary layer and the surface temperature T_w:

$$q(T_w, U_{tot}) = j_w U_{tot} - \frac{j_w}{e}(A - \Delta A + 3.2kT_e), \tag{8}$$

$$j_w(T_w, U_{tot}) = j_{em} + j_{ion} - j_{be}. \tag{9}$$

In Eqs. (8), A is the work function of the electrode material, ΔA is the Shottky correction, T_e is the local electron temperature. The total voltage drop of the near-cathode layer is the total of the voltage drop in the space-charge sheath (U_d) and the voltage drop in the ionization layer (U_i), i.e. $U_{tot}=U_d + U_i$. A similar approach has been applied in [12].

The heat flux $q(T_w,U_{tot})$ and the current density $j_w(T_w,U_{tot})$ serve as boundary conditions of equations (6) and (7). Additionally, losses caused by a black-body radiation of the hot body are considered as $q_r = -\epsilon\sigma_{SB}T^4$. In this way, the electrode is coupled to the LTE plasma column.

The cathode boundary layer is solved prior to the MHD simulation for a series of values of the temperature on the cathode boundary T_w and the voltage drop in the boundary layer U_{tot}. The results are provided as lookup tables and are used during the iterative solution of the combined model.

The consideration of the plasma-anode boundary layer is simpler [13]. The expression for heat fluxes as in many LTE models [3,4] is used in the present work. The normal component of the energy flux to the surface q_a, which is considered additionally to the conductive one, is given by

$$q_a = -\epsilon\sigma_{SB}\ T_w^4\ + |j_e|A_{an}, \tag{10}$$

where ϵ is the emissivity of the surface, σ_{SB} is Stefan-Boltzmann constant, j_e, the electron component of the current density and A_{an} is the work function of the anode material. The term $|j_e|A_{an}$ accounts for heating of the anode caused by the condensation of electrons.

For pure tungsten the work function and the Richardson constant are 4.55 eV and $0.602\cdot10^6$ $Am^{-2}K^{-2}$, respectively. The corresponding values for graphite are 4.6 eV and $0.6\cdot10^6$ $Am^{-2}K^{-2}$, respectively. Melting of the electrodes and metal vapour are not considered in the model.

The model is set up on the commercial computational platform COMSOL Multiphysics® using the interfaces Laminar flow, Electric current, Magnetic field and Heat transfer. The computational domain includes both electrodes and the inter-electrode space in a radial extend of 30 mm. A part of this domain can be seen in Fig. 1. An ambient temperature of 300 K, electric and magnetic insulation are set on the external boundaries. The anode is grounded. The total arc voltage is obtained from an iterative procedure, which ensures that the total electric current equals the given target value.

4. Results

The combined model has been applied to obtain the plasma parameters for arc currents in the range 133-200 A. As a first step, the model of the cathode boundary layer has been validated. This has been done by benchmarking it against results and conditions reported in [11]. The results obtained are shown in Figures 2 and 3. For a fixed value of the total voltage drop U_{tot}=10V, the total current density, its components, total heat flux and its components are obtained. They agree well with the published values. A deviation is found in the voltage drop in the ionization layer U_i for temperatures on the cathode surface above approximately 4000 K, which, however, are not reached in the combined arc simulation, as it is shown below.

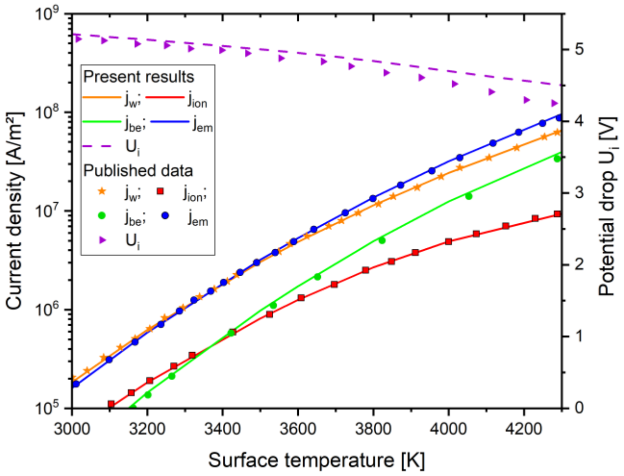

Fig. 2. Total current density and its components in the cathode space-charge sheath for U_{tot} = 10 V.

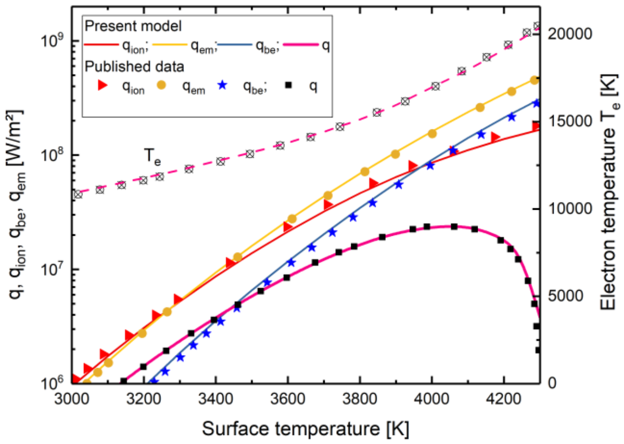

Fig. 3. Total heat flux from the plasma to the cathode surface and its components for U_{tot} = 10 V.

The predicted plasma temperature is compared in Fig.4 with the results from OES in the midplane of the arc (axial position z=2.5 mm) for an arc current of 200 A. The predicted and experimental values are in a good agreement in the arc core. Higher experimental values are observed only for radial positions beyond 5 mm, where a departure from LTE occurs, as it is known from previously published studies. The evaluation for further axial positions in the arc is in progress. The results shown here demonstrate, however, the predictive capability of the model.

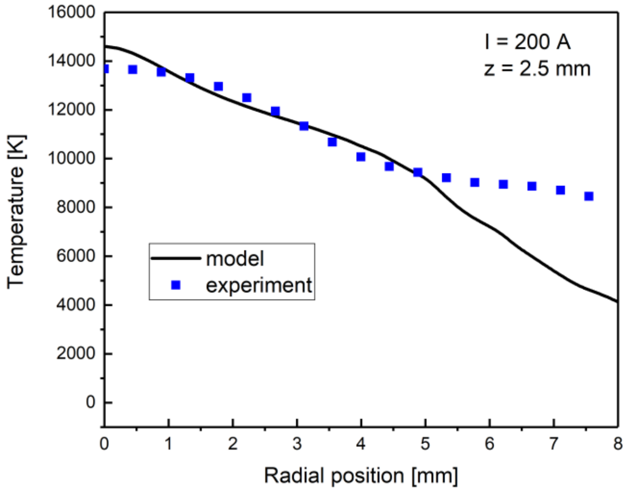

Fig. 4. Radial distribution of the plasma temperature in the midplane of the arc obtained in the combined modelling approach and OES for an arc current 200 A.

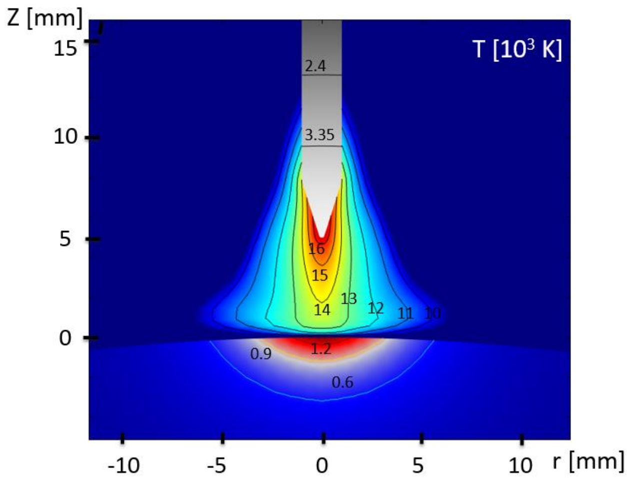

Fig. 5. Two-dimensional distribution of the plasma temperature and the temperature in the electrodes obtained in the combined modelling approach for arc current 200 A.

Fig.5 presents the distribution of the calculated temperature in the plasma and in the electrodes for an current of 200 A. Notice that the temperature for the electrodes is presented with individual scales for a better readability. In the anode body, the temperature reaches maximum values of about 1300 K (well below the melting point of graphite) due to the cooling of the anode bottom surface. In the cathode body, the temperature reaches values of about 4000 K in a restricted part near the cathode tip, where the thermionic emission is strongest. The plasma temperature grows up to about 17000 K close to the cathode tip. Towards the anode the plasma temperature rapidly decreases. The well-known bell-shaped profile of the arc attachment on the anode can be clearly seen.

The importance of the model of the boundary layer is demonstrated in Fig. 6, which presents the plasma temperature and the electric potential obtained in a simple LTE model of the arc column and within the combined modelling approach. The account of the electric power deposited in the cathode boundary layer results in significantly higher plasma temperature not only in the vicinity of the cathode but also in the entire plasma column. This power not only ensures the heating of the cathode and the electron emission needed to sustain the discharge but a part of it goes to the plasma. The higher plasma temperature is related to higher electrical conductivity and to lower voltage drop over the bulk plasma. This in turn leads to an overestimation of the arc voltage in LTE models.

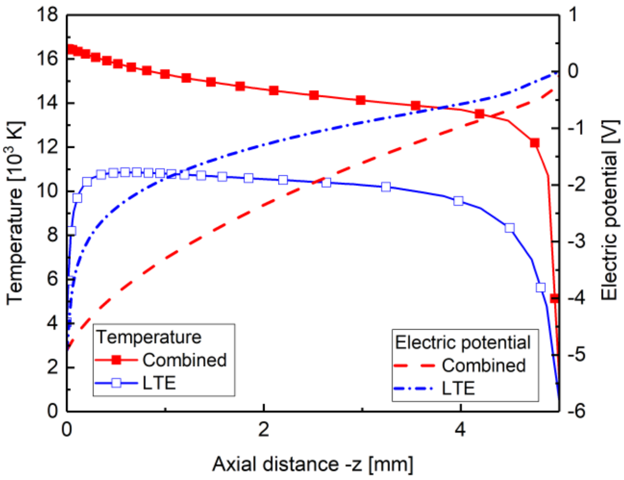

Fig. 6. Plasma temperature and electric potential in the plasma along the arc axis for an arc current of 200 A.

Fig. 7 shows the arc voltage U_{arc} obtained by electric measurements (squares) and the combined modelling approach (line) for arc currents in the range 130-240 A. The good agreement between the modelling and the experimental results is due to the account of the cathode boundary layer in the model. Considering the individual contributions of the boundary layer U_{bl}, the arc column U_{ac}, and the voltage over the cathode body U_c, we see that U_{bl} exceeds by far U_c, although it decreases and U_{ac} increases with the increase of the arc current. The voltage over the cathode body is in the range 0.5-0.75 V and is considerably lower than U_{bl} and U_{ac}. The voltage over the anode body is negligible and is not shown here.

5. Conclusion

In this work, we present the results of experimental and modelling studies on dc electric arc in argon at atmospheric pressure. These studies show that the modelling approach combining the non-equilibrium cathode boundary layer and the LTE arc plasma is capable of predicting the arc plasma temperature and the arc voltage in a good agreement with the experiment. Studies on molecular gases will be considered in future works.

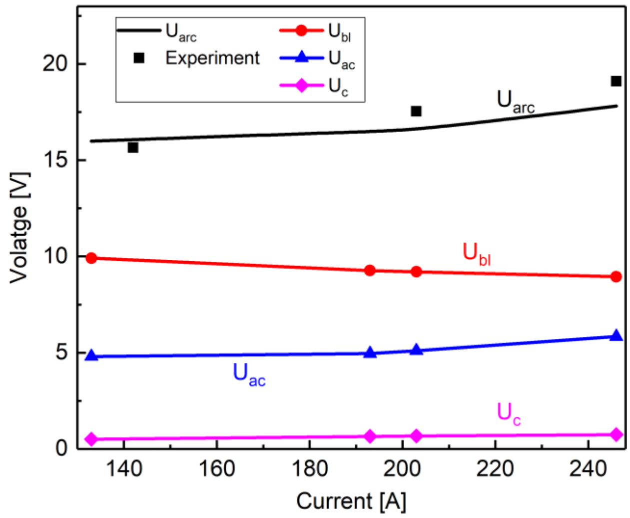

Fig. 7. The current-voltage characteristics of the arc obtained by the combined modelling approach and electric measurements. Additionally, the individual contributions of the boundary layer (U_{bl}), the voltage drop in the cathode (U_c) and the arc column (U_{ac}) are shown.

6. Acknowledgment

This work is carried out at Leibniz Institute for Plasma Science and Technology, Greifswald, with the financial support of the German Academic Exchange Service DAAD, under the Grant number 91644228.

7. References

[1] A.J. Shirvan, I. Choquet, H. Nilsson, J. Phys. D: Appl. Phys. 49 485201 (2016).
[2] M. Lisnyak, M.D. Cunha, J-M Bauchire, M.S. Benilov, J. Phys. D: Appl. Phys. 50 315203 (2017).
[3] J. Lowke, R. Morrow and J. Haidar, J. Phys. D: Appl. Phys. 30 2033–2042 (1997).
[4] L.Sansonnens, J. Haidar, J.J. Lowke, J. Phys. D: Appl. Phys. 33 148– 157 (2000).
[5] M. Baeva , R. Kozakov, S. Gorchakov, D. Uhrlandt, Plasma Sources Sci. Technol. 21 1020-7 (2012).
[6] M. Baeva, M.S. Benilov, N.A. Almeida, D. Uhrlandt, J. Phys. D: Appl. Phys. 49 245205 (2016).
[7] A. B. Murphy, C. J. Arundell, PCPP, 14 451-490 (1994).
[8] A. B. Murphy, PCPP, 15 279-307 (1995).
[9] B. Pateyron, G. Delluc, T&T Winner – Software for thermochemistry, Univ. Limoges, 87051 Limoges Cedex.
[10] M.S. Benilov, A. Marotta, J. Phys D: Appl. Phys., 28 1869-1882 (1995).
[11] M.S.Benilov, M.D. Cunha, J. Phys. D: Appl. Phys. 35 1736-50 (2002).
[12] S. Lichtenberg, L. Dabringhausen, O. Langenscheidt and J. Mentel, J. Phys D: Appl. Phys. 38 3112-3127 (2005).
[13] J. Mentel, J. Heberlein, J. Phys. D: Appl. Phys., 43, 023002 (2010).